

Comparison of Fourier and model-based estimators in single mode multiaxial interferometry

E. Tatulli^{1*} and J.-B. LeBouquin¹

¹*Laboratoire d'Astrophysique, Observatoire de Grenoble, 38041 Grenoble cedex France*

to be inserted later

ABSTRACT

There are several solutions to code the signal arising from optical long baseline multi-aperture interferometers. In this paper, we focus on the **non homothetic spatial coding scheme** (multiaxial) with the fringe pattern coded along one dimension on one detector (all-in-one). After describing the physical principles governing single mode interferometers using that sort of recombination scheme, we analyze two different existing methods that measure the source visibility. The first technique, so-called Fourier estimator, consists in integrating the high frequency peak of the **power** spectral density of the interferogram. The second method, so-called model-based estimator, has been specifically developed for the AMBER instrument of the VLTI and deals with directly modelling the interferogram recorded on the detector. Performances of both estimators are computed in terms of Signal to Noise Ratio (SNR) of the visibility, assuming that the interferograms are perturbed by photon and detector noises. Theoretical expressions of the visibility SNR are provided, validated through numerical computations and then compared. We show that the model-based estimator offers up to 5 times better performances than the Fourier one.

Key words: Techniques:interferometric, Methods:data analysis, Instrumentation:interferometers

1 INTRODUCTION

The next challenge of long baseline optical interferometry is to commonly perform direct imaging of the observed source, the analogous way it is done in radio-interferometry (Högbom 1974) or in infrared aperture masking (Tuthill et al. 2000). After the first promising results obtained with **COAST (Baldwin et al. 1996; Young et al. 2000)**, **NPOI (Hummel 1998)** and **IOTA (Monnier et al. 2004a)**, such technique should soon move one step forward with the operating of the AMBER instrument (Petrov et al. 2000), the three beam re-combiner of the VLTI. From the beginning of 2005, AMBER will indeed take full benefit of the unique combination of the great sensitivity of large aperture telescopes and the spatial frequency coverage provided by the VLTI, even though it will require **multiple nights of observing** to be able to restore consistent images (Thiébaud et al. 2003; Tatulli et al. 2004a). Then, in less than a decade, huge improvements are contemplated to be accomplished with second generation instruments of the VLTI that will enable snapshot imaging by using 4, 6 or even 8 telescopes simultaneously (e.g. **Malbet et al. (2004)**).

One critical point in the design of future interferometric imaging instruments is the choice of the beam recombination scheme, which can become particularly complex, especially when dealing with multi apertures ($N_{tel} \geq 3$) interferometers. Following the solution that has been chosen for the AMBER instrument, we investigate the properties of single mode non-homothetic **spatial coding** scheme (from now on "multiaxial") with all the fringes pattern in the same spatial dimension on the same detector (from now on "all-in-one"). In other words, interferograms are obtained by mixing all together the input beams arising from the different telescopes, thanks to output pupils arranged along one single dimension (see Fig. 1). We analyze the ways to estimate the source visibility from such interferograms.

Indeed, single mode multiaxial all-in-one recombination appears particularly well suited in the framework of interferometric imaging. First it is the simplest and most compact way to recover informations arising from all the baselines. Moreover it provides a better transmission than Michelson recombination schemes (i.e temporal coding) since it makes use of less mirrors and beam splitter for the same given number of input pupils. And the number of pixels required to code the signal is also smaller, which drives to higher limiting magnitudes (Lebouquin et al. 2004). Furthermore, the remarkable spatial filtering properties of single mode

* E-mail: lastname@obs.ujf-grenoble.fr

waveguides allow to change the phase corrugations of the incoming turbulent wavefront into intensity fluctuations at the output of the fibers. In other words, only one fraction of the source flux, so-called coupling coefficient which depends on the Strehl ratio **of the pupil apodized by the fiber single mode** (Coudé du Foresto et al. 2000), remains in the interferogram. But the very advantageous counterpart is that the shape of the interferogram is entirely deterministic, **that is the form of the peaks in the Fourier plane is fixed, and the fringe pattern fully determined by two free parameters, its amplitude and its phase.**

Before the advent of single mode interferometers and in order to overcome the problem of the turbulence, Roddier & Léna (1984) proposed to estimate the visibility in the Fourier plane from the integration of the high frequency peak of the long exposure **power** spectral density of the interferogram. Then Coudé Du Foresto et al. (1997), in a natural way, used the same estimator to compute the visibility arising from the FLUOR experiment, the first interferometer making use of single mode waveguides. In multi-axial coding, we can furthermore take advantage of the deterministic nature of the interferogram shape **to perform model fitting techniques.** It was though only recently, namely for the AMBER instrument, that this property was used to estimate the visibility, by fitting the fringe pattern – **its phase and its amplitude** – in the detector plane (Millour et al. 2004).

In this paper, we recall in Section 2 the general formalism of multi-axial all-in-one recombination, that is the equation governing the interferogram, as well as the two techniques currently used to estimate the visibility. As mentioned above, the first technique, so-called Fourier estimator, integrates the high frequency peak of the **power** spectral density of the interferogram whereas the second one, so-called model-based estimator, directly models the interferogram in the detector plane. For both estimators, theoretical expressions of Signal to Noise Ratio (SNR) of the visibility are provided. In Section 3, those expressions are validated thanks to numerical simulations of noisy interferograms. Then in Section 4 both estimators are compared, from a formal point of view and in terms of relative performances. The influence of instrumental parameters is investigated as well, with a special emphasis regarding the choice of the width of the reading window of the detector. **The presence of atmospheric piston which blurs the fringes has not been taken into account in this analysis. Indeed, regardless the chosen estimator, its effect results in an attenuation of the squared visibility (Colavita 1999), and the sensitivity of both estimators to this point is the same.**

This paper is the first part of our study on multi-axial all-in-one recombination. In a second paper (Lebouquin & Tatulli 2005), we analyze in which way such recombination scheme allows to optimize the visibility SNR thanks to specific geometric configuration of the output pupils.

2 GENERAL FORMALISM

Figure 1 sketches the principle of multi-axial recombination in waveguided interferometers. The light arising from the

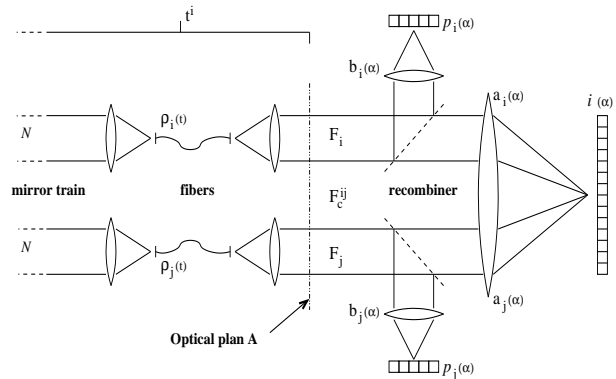


Figure 1. Sketch of a multi-axial all-in-one single mode interferometer. t^i denotes the total "static" transmission from the i^{th} telescope aperture to the optical plane A (i.e. mirrors, delay line, transmission of the i^{th} fiber, ...), whereas ρ^i takes into account the "dynamical" transmission, that is the coupling coefficient of the i^{th} fiber. $i(\alpha)$ is the interferogram. $p^i(\alpha)$ and $p^j(\alpha)$ are the photometric channels. The photometric fluxes F^i , F^j and the coherent flux F_c^{ij} are defined in the optical plane A. $a^i(\alpha)$ and $b^i(\alpha)$ are respectively the detected beams in the interferometric and photometric channels. In other words, $a^i(\alpha)$ and $b^i(\alpha)$ are the transmission factor between the photometric flux and the interferometric and photometric channels, respectively. Note that the definition of $a^i(\alpha)$ and $b^i(\alpha)$ includes the transmission of the beam splitter.

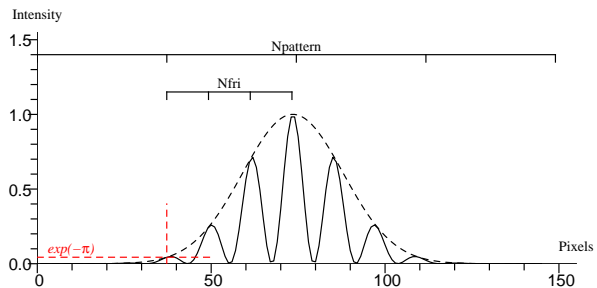


Figure 2. Image of a typical interferogram at the output of multi-axial all-in-one recombining. Here is shown a 2-beam recombination with instrumental contrast set to 1. The fringes are weighted by the **intensity mode pattern** (dashed line). $N_{pattern}$ indicates the width of the detector reading window, the width of one mode pattern being defined as the interval between the top of the Gaussian mode and where the amplitude of the Gaussian mode has decreased by a factor $\exp(-\pi)$. This definition has been chosen so that this width corresponds to half of the first lobe of the Airy pattern in case of pupils which are not weighted by the first mode of single-mode fibers. N_{fri} refers to the number of fringes in one mode pattern. This term is fixed by the distance between the output pupils.

i^{th} telescope is filtered by a single mode fiber to convert phase fluctuations of the corrugated wavefront into intensity fluctuations. The fraction of light ρ^i entering the fiber is called the coupling coefficient (Shaklan & Roddier 1988) and depends on the Strehl ratio **of the apodized pupil** (Coudé du Foresto et al. 2000). Making use of a beam splitter, one part of the light is selected to estimate the photometry, thanks to dedicated photometric channels. The remaining part of the light is recombined with the beam coming

for the j^{th} telescope to form fringes. The coding frequency of the fringes f^{ij} is fixed by the separation of the output pupils, which are arranged along one dimension.

When the only i^{th} beam is lighted, the signal recorded on the interferometric channel is the photometric flux F^i spread on the **intensity mode** pattern $a^i(\alpha)$, that is the diffraction pattern of the i^{th} output pupil weighted by the single mode of the fiber. α is the angular variable in the image plane. F^i results in the source photon flux N attenuated by the total transmission of the instrument, i.e. the product of the "static" transmission t^i and the coupling coefficient ρ^i of the single mode fiber:

$$F^i = N t^i \rho^i \quad (1)$$

When beams i and j are lighted simultaneously, the coherent addition of both beams results in an interferometric component superimposed to the photometric continuum. The interferometric part, that is the fringes, arises from the amplitude modulation of the coherent flux F_c^{ij} at the coding frequency f^{ij} . The coherent flux is the geometrical product of the photometric fluxes, weighted by the visibility:

$$F_c^{ij} = 2N \sqrt{t^i t^j} \sqrt{\rho^i \rho^j} V^{ij} e^{i(\Phi^{ij} + \phi_p^{ij})} \quad (2)$$

where $V^{ij} e^{i\Phi^{ij}}$ is the complex modal visibility (Mège et al. 2001) and ϕ_p^{ij} takes into account a potential differential atmospheric piston. Note that strictly speaking the modal visibility is not the source visibility. **Rigorously, the modal visibility depends on the convolution between the source visibility and the telescope transfer function which is atmosphere dependent in the optical range. As such the modal visibility is biased both by the geometric antenna-lobe effect (the object is multiplied by the telescope point spread function, as commonly known in radio-astronomy), and by the turbulence. When the object is unresolved by one single telescope however, the modal visibility can be fairly approximated by the object one (Tatulli & Chelli 2005) and its estimation is robust (stable to the level of 1% or less) to a change of atmospheric during the calibration process (Tatulli et al. 2004b). In any case, a further study of the relationship between the modal visibility and the source visibility is beyond the scope of this paper, and further informations can be found in papers mentioned above. Here we consider our observable to be the modal visibility.**

Such an analysis can be done for each pair of telescopes available in the interferometer. As a result, the interferogram recorded on the detector can be written in the general form:

$$i(\alpha) = \sum_i^{N_{tel}} a^i(\alpha) F^i + \sum_{i < j}^{N_{tel}} \sqrt{a^i(\alpha) a^j(\alpha)} C_B^{ij}(\alpha) \text{Re} \left[F_c^{ij} e^{i(2\pi \alpha f^{ij} + \phi_s^{ij}(\alpha) + \Phi_B^{ij}(\alpha))} \right]$$

where $\phi_s^{ij}(\alpha)$ is the instrumental phase taking into account possible misalignment and/or differential phase between the beams $a^i(\alpha)$ and $a^j(\alpha)$. C_B^{ij} and $\Phi_B^{ij}(\alpha)$ are respectively the loss of contrast and the phase shift due to diffraction and polarization effects¹, which may not be

homogeneous along the fringe pattern. Fig. 2 gives an example of a multi-axial all-in-one interferogram in the two telescope case.

Thanks to the photometric channels, the number of photoevents $p^i(\alpha)$ coming from each telescope can be estimated independently:

$$p^i(\alpha) = F^i b^i(\alpha) \quad (4)$$

where $b^i(\alpha)$ is the detected beam in the i^{th} photometric channel.

We can notice from Eq.'s (1) and (2) that the estimator of the squared modal visibility $|\widetilde{V^{ij}}|^2$ results in the ratio between the **squared** coherent flux and the photometric fluxes. Using the previous definitions, we can set a generic form of the estimator as following:

$$|\widetilde{V^{ij}}|^2 = \frac{\langle |F_c^{ij}|^2 \rangle}{\langle 4F^i F^j \rangle} \quad (5)$$

Note that $\langle |F_c^{ij}|^2 \rangle$ is computed instead of $\langle F_c^{ij} \rangle$ because in absence of fringe tracking the random atmospheric differential piston ϕ_p^{ij} totally blur the coherent signal. It now remains to estimate F^i and F_c^{ij} from the interferogram.

2.1 Fourier estimator: integrating the power spectral density

In the Fourier space, the interferogram defined by Eq. (3) takes the form of the sum of photometric and interferometric peaks. The photometric peaks are centered at the zero spatial frequency whereas the interferometric peaks $\widehat{M}_+^{ij}(f)$ are located at their respective spatial coding frequency f^{ij} , their counterpart $\widehat{M}_-^{ij}(f)$ being in the negative spatial frequency domain. This method in the Fourier space requires that (i) the photometric peaks and the interferometric peaks are not overlapping, and, (ii) the high frequency peaks are not overlapping between each other. If these conditions are fulfilled, the squared coherent flux can be estimated by computing the integral of the power spectral density $|\widehat{M}_+^{ij}(f)|^2$ (Roddier & Léna 1984; Conan 1994), over its frequency support, that is $[f^{ij} - D/\lambda, f^{ij} + D/\lambda]$ where D is the diameter of the output pupil. From the definition of the coherent flux and using the Parseval equality, it comes:

$$\int |\widehat{M}_+^{ij}(f)|^2 df = |F_c^{ij}|^2 \frac{\int C_B^{ij2}(\alpha) a^i(\alpha) a^j(\alpha) d\alpha}{4} \quad (6)$$

The photometric flux is easily computed from the photometric channel (see Eq. (4)):

$$\widehat{P}^i = F^i \int b^i(\alpha) d\alpha \quad (7)$$

Then the estimation of the fringe contrast C^{ij} writes:

$$|\widetilde{C^{ij}}|^2 = \frac{\langle \int |\widehat{M}_+^{ij}(f)|^2 df \rangle}{\langle \widehat{P}^i \widehat{P}^j \rangle} = |\widetilde{V^{ij}}|^2 \cdot C_r^2 \quad (8)$$

with

$$C_r^2 = \frac{\int C_B^{ij2}(\alpha) a^i(\alpha) a^j(\alpha) d\alpha}{\int b^i(\alpha) d\alpha \int b^j(\alpha) d\alpha} \quad (9)$$

being the instrumental contrast of the recombiner that depends on the contrast loss due to polarization effects,

¹ assuming a non-polarized incoming light

on the alignment of the beams $a^i(\alpha)$ and $a^j(\alpha)$, and on the flux ratio between the interferometric and the photometric channels. Note that the **power** spectral density of the interferogram has to be properly unbiased from photon and detector noise (Perrin 2003).

2.2 Model-based estimator: modelling the interferogram

The model-based estimator has been introduced for the first time in the data reduction process of the AMBER instrument (Millour et al. 2004). It consists in modelling the interferogram thanks to *a priori* knowledges of the instrument. The purpose of such a signal processing is twofold: (i) to develop optimized algorithms in terms of performances of the instrument, that is the SNR of the visibility; and (ii) on the contrary of the Fourier estimator, to authorize high frequency peak overlapping when dealing with multi-beam ($N_{tel} > 3$) recombination, thus allowing to code the interferogram on less pixels. This second point is beyond the scope of this paper. Let just mention here that plainly choosing the different coding frequencies is crucial to design optimized multi-beam recombiner making use of integrated optics. This is especially true in the case of imaging instruments such as VITRUV (Lebouquin et al. 2004) that are recombining 4 beams or more, as it is shown in our second paper on the subject (Lebouquin & Tatulli 2005).

A full description of this estimator can be found in Millour et al. (2004). We only recall here the basics principles. To model the signal on the detector, Eq. (3) has to be rewritten in its sampled version, where k stands for the pixel number, between 1 and N_{pix} :

$$i_k = \sum_i^{N_{tel}} F^i a_k^i + \sum_{i < j}^{N_{tel}} c_k^{(i,j)} R^{ij} + d_k^{(i,j)} I^{ij} \quad (10)$$

with

$$c_k^{(i,j)} = \frac{C_B^{ij}(k) \sqrt{a_k^i a_k^j}}{\sqrt{\sum_k C_B^{ij^2}(k) a_k^i a_k^j}} \cos(2\pi \alpha_k f^{ij} + \phi_s^{ij}(k) + \Phi_B^{ij}(k)) \quad (11)$$

and

$$R^{ij} = \sqrt{\sum_k C_B^{ij^2}(k) a_k^i a_k^j} \text{Re} [F_c^{ij}] \quad (12)$$

$d_k^{(i,j)}$ and I^{ij} being the quadratic counterpart of $c_k^{(i,j)}$ and R^{ij} respectively. $c_k^{(i,j)}$ and $d_k^{(i,j)}$ are called the carrying waves of the signal at the coding frequency f^{ij} , since they "carry" (in terms of amplitude modulation) R^{ij} and I^{ij} , which are directly linked to the complex coherent flux. Furthermore, the photometric fluxes are still computed from the photometric channels (see Eq. (7)):

$$p^i = F^i \sum_k b_k^i \quad (13)$$

F^i and F_c^{ij} are then jointly estimated from the photometry (p^i) and the interferogram (i_k) by resolving a set of ($N_{pix} + N_{tel}$) linear equations with $(2N_b + N_{tel})$ unknowns (N_b being the number of pairs of telescopes, i.e. $N_b = N_{tel}(N_{tel} - 1)/2$):

$$\begin{bmatrix} i \\ p \end{bmatrix} = [\mathbf{C}] \cdot \begin{bmatrix} R \\ I \\ F \end{bmatrix} \quad (14)$$

where the matrix \mathbf{C} takes the detailed form:

$$\begin{pmatrix} \overbrace{\dots}^{N_b} & \overbrace{\dots}^{N_b} & \overbrace{\dots}^{N_{tel}} \\ \dots & \dots & \dots \\ \dots & \dots & \dots \\ \dots & \dots & \dots \\ \dots & \dots & \dots \\ \dots & \dots & \dots \\ \dots & \dots & \dots \\ \dots & \dots & \dots \\ \dots & \dots & \dots \\ \dots & \dots & \dots \end{pmatrix} \quad (15)$$

The matrix \mathbf{C} entirely characterizes the instrument. It depends on the shape of the detected beams a_k^i , b_k^i and on the carrying waves $c_k^{(i,j)}$, $d_k^{(i,j)}$ that hold informations about the interferometric beam $\sqrt{a_k^i a_k^j}$, the coding frequencies f^{ij} and the instrumental differential phases ϕ_s^{ij} , and the polarization state within C_B^{ij} and Φ_B^{ij} . Such quantities can be calibrated in laboratory, hence they are assumed to be perfectly known. The calibration procedure is fully described by Millour et al. (2004). \mathbf{C} has to be inverted in order to solve the system. In the AMBER experiment, the generalized inverse of \mathbf{C} has been called the Pixel To Visibility Matrix (P2VM), since it enables to compute the visibility of the fringes from the measurements on the detector. The estimation of the contrast writes:

$$|\widetilde{V^{ij}}|^2 = \frac{\langle R^{ij^2} \rangle + \langle I^{ij^2} \rangle}{\langle p^i p^j \rangle} = |\widetilde{V^{ij}}|^2 \cdot C_r^2 \quad (16)$$

C_r^2 is still the squared instrumental contrast:

$$C_r^2 = \frac{\sum_k C_B^{ij^2}(k) a_k^i a_k^j}{\sum_k b_k^i \sum_k b_k^j} \quad (17)$$

with the same definition than in Eq. (9). Note that the quantity $R^{ij^2} + I^{ij^2}$ has to be properly unbiased, like the **power** spectral density in the Fourier plane.

2.3 SNR of the modal visibility

Using second order expansion of Papoulis (1984), we derive from Eq. (5) the relative error (i.e. the inverse of the SNR) of the squared visibility:

$$\begin{aligned} \mathcal{E}^2(|V^{ij}|^2) &= \frac{\sigma^2(|F_c^{ij}|^2)}{|F_c^{ij}|^2} + \frac{\sigma^2(F^i)}{F^i^2} + \frac{\sigma^2(F^j)}{F^j^2} \\ &+ 2 \frac{\text{Cov}(F^i, F^j)}{F^i F^j} - 2 \frac{\text{Cov}(|F_c^{ij}|^2, F^i F^j)}{|F_c^{ij}|^2 F^i F^j} \end{aligned} \quad (18)$$

The main difference between both approaches lies in the following remark: in the case of the Fourier estimator, the coherent and photometric fluxes are directly estimated from the measurements, each *independently*, whereas in the case of the model-based estimator, the coherent and photometric fluxes are *jointly* reconstructed from the measurements by way of computation of the P2VM matrix, and are therefore correlated. As a result we have the following situations:

Fourier estimator	Model-based estimator
$\text{Cov}(F_c^{ij} ^2, F^i F^j) = 0$ $\text{Cov}(F^i, F^j) = 0$	$\text{Cov}(F_c^{ij} ^2, F^i F^j) \neq 0$ $\text{Cov}(F^i, F^j) \neq 0$

Detailed computation of Eq. (18) are given in Appendix A for both estimators, assuming that the interferogram is corrupted by photon and detector noise. Atmospheric noise is neglected here since it has been shown in Tatulli et al. (2004b) that in presence of **modal filtering – and on the contrary of multispeckle interferometry (Goodman 1985) –, speckle noise is the dominant noise in the case of very bright sources (negative magnitudes) only, and is therefore marginally relevant. Furthermore, we did not take into account in these computations the effect of atmospheric piston since it only results in the attenuation of the squared visibility, the sensitivity of both estimators to this specific point being the same.**

In next section, we propose to simulate the estimation of the modal visibility from multi-axial recombination and to validate our theoretical calculations. Then we compare the performances of both estimators.

3 VALIDATION OF THE THEORETICAL EXPRESSIONS

In order to validate our theoretical expressions derived in the previous section, we perform statistical simulations of noisy interferograms. For sake of simplicity we assume from now on a two telescope interferometer. Note however that the validity of our theoretical approach has been also checked for increasing number of telescopes. Moreover, a deep analysis of multi-beam (≥ 3) recombination is proposed in our second paper on the subject (Lebouquin & Tatulli 2005).

Following the formalism of Section 2, the interferogram arising from multi-axial all-in-one recombination is entirely defined by the following parameters:

(i) The shape of $a(\alpha)$, which is assumed to be the same for each beam. It arises from the inverse Fourier Transform of the auto-correlation of the output pupil of diameter D . **To take into account the weighting of the single mode fiber we assumed a Gaussian shape with a pupil stop of width D (that is a convolution by a Bessel function in the detector plane). As a result, the low and high frequency peaks have truncated Gaussian shapes with a base width of $2D/\lambda$.** We consider that the photometry is recorded on one pixel.

(ii) The number of fringes N_{fri} in the interference pattern for the lowest coding frequency. It is defined as the distance between the closest output pupils in D/λ units (see Fig. 2). We choose here $N_{fri} = 2$.

(iii) The number of pixels per fringe N_{pf} to code the interferogram. It must be chosen such that it fulfills the Shannon criteria for the highest frequency coding f_{max} of the carrying waves. If it is written under the form $f_{max} = \beta D/\lambda$, then the number of pixels must verify: $N_{pf} \geq 2\beta$. For the two telescope case considered here, we arbitrarily set $N_{pf} = 2.5$.

(iv) The width of the detector reading window $N_{pattern}$ which fixes the total number of fringes taken into account in the interferogram and hence the total number of pixels N_{pix}

read on the detector. We impose in this section $N_{pattern} = 2$. This choice means that the detector reading window is **two mode patterns wide, exactly as if we only would consider the fringes in the first lobe of the diffraction pattern, in the case of an Airy disk.** Such choice seems reasonable at first thought since outside this lobe the interferogram is severely attenuated (as one can notice in Fig. 2). Nevertheless, a deeper analysis of this specific point shows that such a parameter is a key issue, as it will be discussed in Section 4.2.

(v) The fraction of flux going into the photometric channels (that is the transmission of the beam splitter). We assume here that the beam-splitter selects 30% of the flux for the photometry.

For a given source magnitude, the number of photoevents occurring on each pixel of the interferometric and the photometric channels are computed following Eq.'s (3) and (4) respectively, assuming photon noise and additive detector noise with $\sigma = 15e^-/\text{pix}$. Such a procedure is then repeated until we obtain a sample of 1000 data sets, which is large enough to perform statistics. For both estimators, we compute theoretical and statistical mean value and Signal to Noise Ratio of the modal visibility $|\widetilde{V^{ij}}|^2$, thanks to Eq.'s (5) and (18). Fig. 3 shows the results of our computations, for both methods (formal and simulated) and for both estimators (P2VM and Fourier), setting the true value of the modal visibility to 0.5. Theoretical calculations and numerical simulations are in excellent agreement, both for the estimated visibility and the SNR. This study validates the theoretical expressions of both estimators as well as their respective theoretical SNR.

4 DISCUSSION

4.1 Estimator relative performances

Although both estimators arise from the same formal definition of Eq. (5), they exhibits fundamental conceptual differences. Obviously, both techniques presents the same instrumental contrast (see Eq.'s (9) and (17) respectively), which is not surprising since the instrumental design is strictly the same, as well as the same estimation of the photometry (see Eq.'s (7) and (13) respectively). However the very difference lies in the computation of the coherent flux.

First, in the Fourier case, the coherent flux results in a second order (i.e. quadratic) estimation, that is $|F_c^{ij}|^2$ is directly estimated. On the contrary, the model-based computation is equivalent to a first order estimation, that is the complex quantity F_c^{ij} is calculated, and then the squared modulus is taken to get rid of the atmospheric differential piston. **This latter method is equivalent to fit the complex Fourier Transform of the interferogram. A second order estimator based on modelling would have been the fitting of the power spectral density itself, or equivalently, the fitting of the auto-correlation of the interferogram in the detector plane. Performing first order estimation is above all interesting because it allows to separate informations (i.e. the visibilities for each baseline) before computing the modulus square. As a result,**

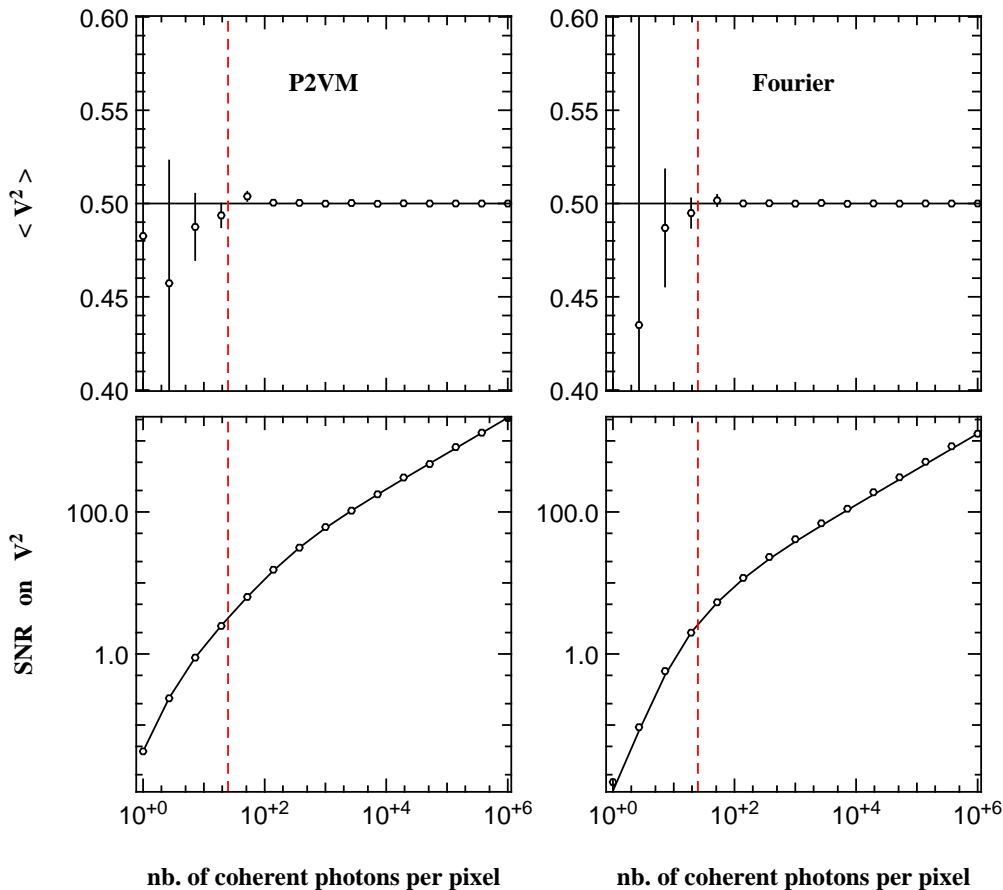


Figure 3. Theoretical (solid lines) and simulated (cross) values of the modal visibility mean value (top) and SNR (bottom), for the P2VM (left) and the Fourier (right) estimators. Plots are shown as a function of the number of photoevents per pixel in the interferogram. Detector noise has been set to $\sigma = 15e^-/\text{pix}$. The vertical dashed line shows the limit between the detector and the photon noise regime. For the estimation of the visibility arising from numerical simulations, we plot the statistical error bars due to limited number of samples (1000 data sets), that is the dispersion of the 1000 estimated modal visibility, divided by the square root of the number of samples.

this method prevents “cross-talk” between the baselines even if the peaks are partially superimposed, which is particularly worthwhile in the case of visibility estimation from multi-beam (≥ 3) interferometers, as developed in our second paper on the subject (Lebouquin & Tatulli 2005). We also infer that a first order estimation drive to better – or at worst identical – performances than quadratic one, though a thorough analysis of this point, which is beyond the scope of this paper, remains to be done. Moreover and above all, the model-based algorithm, thanks to the P2VM calibration matrix, takes entire benefit of the knowledge of the instrument whereas the Fourier estimator does not¹. When making use of the model-based estimator, the shape of the interferogram is perfectly known, precisely its envelope (the diffraction pattern $\sqrt{a_k^i a_k^j}$) as well as its coding frequency and its instrumental phase. These *a priori* informations are gathered in the matrix \mathbf{C} defined in Section 2.2. And clearly, introducing perfectly known (i.e true and un-noisy) *a priori* in the data reduction procedures can

only improve the performances of the corresponding estimator. These two remarks, and particularly the second point, explain why the model-based algorithm leads to better performances than the Fourier one, as it is illustrated in Figure 4. Note that the SNR improvement is all the more important than the visibility is high. In the two telescopes case, a gain of a factor 3 to 5 can be achieved at best, for unresolved sources.

However this analysis assumes perfect calibration of the instrument. It means that the calibration matrix must be both perfectly stable in time and very precise, that is recorded with a SNR much higher than the SNR of the interferograms. If the instrument is not stable between the calibration procedures and the observations, the P2VM will drift and as a result, the estimated visibilities will be biased. And if the calibration is not precise enough, it will be the limiting factor of the visibility SNR. In the case of the AMBER instrument, the calibration procedure is quite complex and it can require a consequent integration time (several minutes) to get a useful and precise calibration. More generally, the time and the way to calibrate an instrument severely depends on its stability and on its complexity. Ambitious designs such as the “silicon v-groove array” of the MIRC recombiner (Monnier et al. 2004b), or recombination schemes

¹ although some approximate assumptions about the peak position have to be made to set the integration interval.

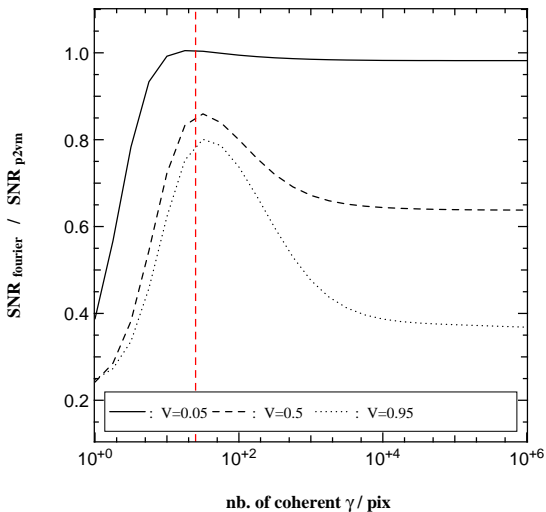


Figure 4. Ratio between the SNR of the Fourier estimator and the SNR of the model-based one, as a function of the number of photoevents per pixel in the interferogram. Detector noise is still $\sigma = 15e^-/\text{pix}$. The curves are plotted for 3 types of sources: fully resolved ($V = 0.05$, solid line), moderately resolved ($V = 0.5$, dashed line) and unresolved ($V = 0.95$, dotted line).

making use of integrated optics chips (Berger et al. 2003; Lebouquin et al. 2004) should drive to drastic improvements on this specific point.

4.2 Influence of instrumental parameters

Previous analysis has been done with a given configuration of the instrument. One last point to investigate is how both estimator behave, one compare to the other, when the parameters governing the interferogram are varying. Obviously, modifying the number of pixel per fringe or even the detector noise level will result in similar changes for both estimators, that is the slope of the SNR in the detector noise regime. As well, changing the coding frequency, which only defines the position of the interferometric peak in the Fourier space, will lead to equivalent modifications of both estimators performances, at least as far as the high frequency peaks are separable². At last, choosing the optimized area on which the interferogram gives valuable informations without adding too much detector noise is a crucial point. Since the model-based algorithm takes into account the shape of the interferogram whereas the Fourier estimator does not, the compromise to find is not the same in both cases. It means the response to a change of the detector reading window will differ with regards to the chosen estimator. The effects of this parameter are investigated here.

In a multiaxial combination, one has the choice of the limits of the reading window on the detector, i.e of the number of pixels to consider. And the largest the window, the more signal you integrate, but the more detector noise you record too. In Figure 5, we show the evolution of the SNR ratio of the modal visibility as a function of the width of the window on the detector (here defined in fraction of **intensity mode** pattern). The entire first lobe of the fringe

pattern contains $N_{fri} = 8$ fringes, with $N_{pf} = 4$ pixels per fringe. All the other parameters of the instrument are kept unchanged.

Fourier estimator: In the photon poor regime, at the detection limit of the instrument, the SNR shows a maximum when the width of the reading window is about half of the first lobe of the envelope. Beyond that point, the pixels have very small individual SNR and only bring a noise contribution in the estimation of the visibility. In the photon rich regime, the SNR reaches its maximum for the same width of the reading window but exhibits a plateau as the width increases. This behavior stands as long as the SNR of each individual pixel is dominated by the photon noise. Then the SNR of the visibility starts to decrease. The width of the plateau depends on the incoming flux of the source and is all the more large than the source is bright.

Model-based estimator: As for the Fourier estimator, the shape of the SNR is linked to the shape of the fringe pattern. But in this case, the SNR is increasing with the width of the detector window and does not exhibit a maximum (in other word, the optimal is found for an "infinite" width). As a matter of fact, thanks to the generalized inverse of the matrix \mathbf{C} that takes into account the shape of the interferogram, each pixel contribution is weighted by its individual SNR. So the pixels with bad SNR (due to the envelope or fringe modulation) are "removed" from the reconstruction and do not introduce noise in the estimation of the visibility. Nevertheless, we can see that the slope of the SNR becomes almost flat from a detector width of about one **intensity mode** pattern.

This analysis shows that, in the framework of interferometric observations making use of multiaxial all-in-one recombination, and in the case of bright sources, it is worth the effort to integrate the **interferogram on the entire lobe** in order to optimize the SNR of the visibility. This statement stands for both estimators. When observing faint sources, that is when reaching the limiting magnitude of the instrument, and in the specific case of the Fourier estimator, performances are slightly improved when reducing the width of the reading window to half of the lobe, although the gain on the SNR never exceed a factor of 2.

5 CONCLUSION

In this paper, we have developed the theoretical formalism that allows to model single mode interferometers using multiaxial all-in-one-coding, from the signal processing point of view. From this formalism, two estimators of the visibility have been analyzed. The first one consist in using the classical integration of the **power** spectral density of the interferogram in the Fourier plane whereas the second one deals with modeling the interferogram in the detector plane, as it has been chosen for the AMBER experiment. Performances of such estimators have been computed. Considering photon and detector noises, theoretical expression of the SNR of the visibility have been recalled for the Fourier estimator, and derived for the first time in the case of model-based estimators. These expressions have been validated through numerical simulations and then compared. We have shown that the second technique offers optimal performances since it makes full use of knowledges about the instrument, especially the

² when $N_{tel} \geq 3$, see Lebouquin & Tatulli (2005)

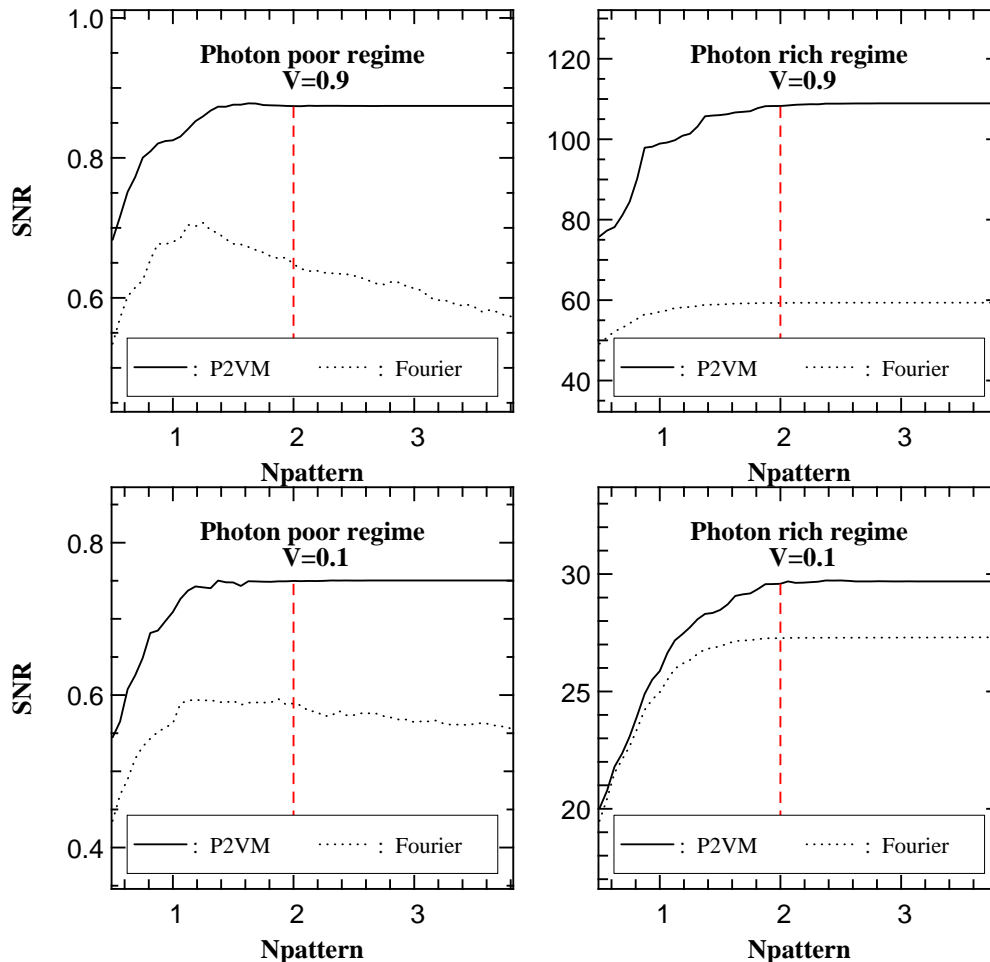


Figure 5. SNR of the modal visibility as a function of the detector reading window, in fraction of **intensity mode** pattern, for photon poor (left, here $1\gamma/\text{pix}$) and photon rich (right, here $10^6\gamma/\text{pix}$) regimes. Results are displayed for marginally resolved ($V = 0.9$, top) and fully resolved ($V = 0.1$, bottom) sources. The instrumental parameters are: $N_{\text{fri}} = 4$ fringes per beam, $N_{\text{pf}} = 4$ pixels per fringe, and a detector noise of $\sigma = 15e^-/\text{pix}$. The vertical dash lines correspond to recording one entire mode pattern (see Fig. 2).

shape of the interferogram. In the two telescopes case which has been emphasized in this paper, we have demonstrated that the model-based estimator enables at best to come over a factor of 5 of the visibility SNR, compare to the Fourier one. Finally we have addressed the question of the width of the reading window of the detector. This point is indeed a crucial issue when dealing with multiaxial recombination. We have shown that, regardless of the chosen estimator, integrating the entire lobe of the intensity mode pattern offers optimized performances.

ACKNOWLEDGMENTS

Authors thank Drs K. Perrault and F. Malbet for very helpful suggestions that improved the presentation of the paper. They wish also to thank the referee for its careful reading of this work and its subsequent comments that made this paper much clearer. All the calculations and graphics were performed with the freeware *Yorick*²

REFERENCES

- Baldwin, J. E., et al. 1996, *Astron. & Astrophys.*, 306, L13
- Berger J., et al., 2003, *Proc. SPIE*, 4838, 1099
- Colavita, M. M. 1999, *Public. of the Astron. Soc. Pac.*, 111, 111
- Conan J.-M., 1994, Ph.D. Thesis, Univerté Paris XI Orsay
- Coudé du Foresto V., Faucherre M., Hubin N., Gitton P., 2000, *A&AS*, 145, 305
- Coude Du Foresto V., Ridgway S., Mariotti J.-M., 1997, *A&A Suppl. Ser.*, 121, 379
- Goodman J. W., 1985, *Statistical Optics*, New York: Wiley, 1985
- Högbom J. A., 1974, *A&AS*, 15, 417
- Hummel C. A., 1998, *Proc. SPIE*, 3350, 483
- Lebouquin J.-B., Berger J.-P., Labeye P., et al., 2004, *Proc. SPIE*, 5491, 1362
- Lebouquin J.-B. Tatulli E., 2005, *MNRAS*, in prep.
- Malbet, F., Berger, J.-P., Kern, P., et al. 2004, *Proc. SPIE*, 5491, 439
- Mège P., Malbet F., Chelli A., 2001 in SF2A-2001: Semaine de l’Astrophysique Francaise, eds. F. Combes, D. Barret, and F. Thévenin, EDP Sciences, p. 581

² <ftp://ftp-icf.11nl.gov/pub/Yorick/doc/index.html>

- Millour F., Tatulli E., Chelli A., et al., 2004, Proc. SPIE, 5491, 1222
- Monnier J. D., et al., 2004, ApJ, 602, L57
- Monnier J. D., et al., 2004, Proc. SPIE, 5491, 1370
- Papoulis A., 1984, Probability, random variables and stochastic processes, New York: McGraw-Hill, 2nd ed.
- Perrin G., 2003, A&A, 398, 385
- Petrov R. G., Malbet F., Richichi A., et al., 2000, Proc. SPIE, 4006, 68
- Roddiar F., Lena P., 1984, Journal of Optics, 15, 171
- Shaklan S., Roddiar F., 1988, ApOpt, 27, 2334
- Tatulli E., Mège P., Chelli A., 2004, A&A, 418, 1179
- Tatulli E., Thiébaud E., Malbet F., Duvert G., 2004, Proc. SPIE, 5491, 117
- Tatulli, E., & Chelli, A. 2005, Optical Society of America Journal A, 22, 1589
- Thiébaud E., Garcia P. J. V., Foy R., 2003, Ap&SS, 286, 171
- Tuthill P. G., Monnier J. D., Danchi W. C., 2000, Proc. SPIE, 4006, 491
- Young J. S., et al., 2000, MNRAS, 315, 635

APPENDIX A: THEORETICAL SNR OF THE VISIBILITY

We assume that the interferogram as well as the photometric outputs are corrupted by photon (Poisson) noise and additive Gaussian noise of variance σ^2 .

A1 Generic expression

The estimator of the square visibility can be expressed in a generic form:

$$\widetilde{|V^{ij}|^2} \propto \frac{\langle |F_c^{ij}|^2 \rangle}{\langle F^i F^j \rangle} \quad (\text{A1})$$

where F_c^{ij} the coherent flux at the frequency f^{ij} , an F^i , F^j are the photometric fluxes.

The relative error $\mathcal{E}(|V^{ij}|^2)$ on the square visibility is then given by Papoulis (1984):

$$\begin{aligned} \mathcal{E}^2(|V^{ij}|^2) &= \frac{\sigma^2(|F_c^{ij}|^2)}{|F_c^{ij}|^2} + \frac{\sigma^2(F^i)}{F^i{}^2} + \frac{\sigma^2(F^j)}{F^j{}^2} \\ &+ 2 \frac{\text{Cov}(F^i, F^j)}{F^i F^j} - 2 \frac{\text{Cov}(|F_c^{ij}|^2, F^i F^j)}{|F_c^{ij}|^2 F^i F^j} \quad (\text{A2}) \end{aligned}$$

Theoretical expression of each term of previous equation is now given for both estimators.

A2 SNR for the Fourier estimator

The coherent flux is linked to the spectral density of the interferogram by the following relationship (see Eq. (6), written in its sampled form):

$$|F_c^{ij}|^2 \propto \sum_k |\widehat{M}^{ij}(f_k)|^2 \quad (\text{A3})$$

Hence the expected value and the error on the coherent flux writes:

$$\overline{|F_c^{ij}|^2} \propto \sum_k \overline{|\widehat{M}^{ij}(f_k)|^2} \quad (\text{A4})$$

$$\begin{aligned} \sigma^2(|F_c^{ij}|^2) &\propto \sum_k \sigma^2(|\widehat{M}^{ij}(f_k)|^2) + \\ &\sum_k \sum_{l \neq k} \text{Cov}(|\widehat{M}^{ij}(f_k)|^2, |\widehat{M}^{ij}(f_l)|^2) \quad (\text{A5}) \end{aligned}$$

The statistics of the spectral density of an interferogram have already been computed by Goodman (1985) in the case of photon noise and completed by Tatulli et al. (2004b) with detector and atmospheric noise. We recall the results here, without taking into account the atmospheric noise (i.e. speckle noise):

$$\overline{|\widehat{M}^{ij}(f_k)|^2} = \overline{N}^2 |\widehat{i}(f_k)|^2 + \overline{N} + N_{pix} \sigma_{det}^2 \quad (\text{A6})$$

where we recognize the bias part due to photon noise (\overline{N} , Goodman (1985)) and additive Gaussian noise ($N_{pix} \sigma_{det}^2$, Tatulli et al. (2004b)),

$$\begin{aligned} \sigma^2(|\widehat{M}^{ij}(f_k)|^2) &= 2\overline{N}^3 |\widehat{i}(f_k)|^2 + 4\overline{N}^2 |\widehat{i}(f_k)|^2 + \overline{N}^2 + \\ &N_{pix}^2 \sigma^4 + 3N_{pix} \sigma^4 + 2N_{pix} \sigma^2 \overline{N} + \\ &2N_{pix} \sigma^2 \overline{N}^2 |\widehat{i}(f_k)|^2 \quad (\text{A7}) \end{aligned}$$

$$\begin{aligned} \text{Cov}(|\widehat{M}^{ij}(f_k)|^2, |\widehat{M}^{ij}(f_l)|^2) &= 2\overline{N}^3 \text{Re} \left[\widehat{i}(f_k) \widehat{i}^*(f_l) \widehat{i}^*(f_k - f_l) \right] + \\ &2\overline{N}^3 \text{Re} \left[\widehat{i}(f_k) \widehat{i}(f_l) \widehat{i}^*(f_k + f_l) \right] + 2\overline{N}^2 |\widehat{i}(f_k)|^2 + 2\overline{N}^2 |\widehat{i}(f_l)|^2 + \\ &\overline{N}^2 |\widehat{i}(f_k - f_l)|^2 + \overline{N}^2 |\widehat{i}(f_k + f_l)|^2 + \overline{N} + 3N_{pix} \sigma^4 \quad (\text{A8}) \end{aligned}$$

where $\widehat{i}(f)$ is the normalized spectral density (such as $\widehat{i}(0) = 1$), that is:

$$\widehat{i}(f) = V(f) \widehat{g}(f) \quad (\text{A9})$$

$$\widehat{i}(f) = \frac{V(f)}{N_{tel}} \widehat{g}(f) \quad (\text{A10})$$

for the photometric and the interferometric peaks respectively, N_{tel} being the number of telescopes, and $\widehat{g}(f)$ being the normalized Fourier Transform of the beam $a(\alpha)$ (assuming, the same shape for the whole beams). Furthermore, we have

$$\sigma^2(F^i) = \overline{F^i} + \sigma_{det}^2 \quad (\text{A11})$$

Finally, since the coherent flux and each photometric flux are estimated independently, we have:

$$\text{Cov}(|F_c^{ij}|^2, F^i F^j) = 0 \quad (\text{A12})$$

$$\text{Cov}(F^i, F^j) = 0 \quad (\text{A13})$$

A3 SNR for the P2VM estimator

We recall that the real and imaginary part of the weighted complex visibility are defined by the system of equations:

$$\begin{bmatrix} i \\ P \end{bmatrix} = [C] \cdot \begin{bmatrix} R \\ I \\ F \end{bmatrix} \quad (\text{A14})$$

if we call $\mathbf{M} = m_k, k \in [1..N_{pix} + N_{tel}]$ the vector resulting in the concatenation of the interferogram i and the photometry P , we can write:

$$R^{ij} = \sum_k^{N_{pix}} \xi_k^{ij} m_k \quad (\text{A15})$$

$$I^{ij} = \sum_k^{N_{pix}} \zeta_k^{ij} m_k \quad (\text{A16})$$

$$F^i = \sum_k^{N_{pix}} \beta_k^i m_k \quad (\text{A17})$$

where ξ_k^{ij}, ζ_k^{ij} and β_k^i are the coefficients of the P2VM matrix. Hence it comes:

$$|F_c^{ij}|^2 = R^{ij2} + I^{ij2} = \sum_k \sum_l [\xi_k^{ij} \xi_l^{ij} + \zeta_k^{ij} \zeta_l^{ij}] m_k m_l \quad (\text{A18})$$

$$F^i F^j = \sum_k \sum_l \beta_k^i \beta_l^j m_k m_l \quad (\text{A19})$$

Here, the covariance between the coherent flux and the photometric fluxes, as well as the covariance between the photometric fluxes have to be taken into account. For sake of simplicity, Eq. (A2) can be rewritten:

$$\mathcal{E}^2(|V^{ij}|^2) = \frac{\sigma^2(|F_c^{ij}|^2)}{|F_c^{ij}|^2} + \frac{\sigma^2(F^i F^j)}{F^i F^j} - 2 \frac{\text{Cov}(|F_c^{ij}|^2, F^i F^j)}{|F_c^{ij}|^2 F^i F^j} \quad (\text{A20})$$

It now remains to compute all the terms knowing that:

$$\sigma^2(|F_c^{ij}|^2) = \overline{|F_c^{ij}|^4} - \overline{|F_c^{ij}|^2}^2 \quad (\text{A21})$$

$$\sigma^2(F^i F^j) = \overline{F^{i2} F^{j2}} - \overline{F^i F^j}^2 \quad (\text{A22})$$

$$\text{Cov}(|F_c^{ij}|^2, F^i F^j) = \overline{|F_c^{ij}|^2 F^i F^j} - \overline{|F_c^{ij}|^2} \overline{F^i F^j} \quad (\text{A23})$$

To lighten the calculations we introduce the variable γ such that $\gamma_{kl}^{ij} = \xi_k^{ij} \xi_l^{ij} + \zeta_k^{ij} \zeta_l^{ij}$. Then we can compute the second order statistics of the square coherent flux and the photometric fluxes:

$$\overline{|F_c^{ij}|^2} = \sum_k \sum_l \gamma_{kl}^{ij} \overline{m_k m_l} = \sum_k \gamma_{kk}^{ij} \overline{m_k^2} + \sum_k \sum_{l \neq k} \gamma_{kl}^{ij} \overline{m_k} \overline{m_l} \quad (\text{A24})$$

$$\overline{F^i F^j} = \sum_k \beta_k^i \beta_k^j \overline{m_k^2} + \sum_k \sum_{l \neq k} \beta_k^i \beta_l^j \overline{m_k} \overline{m_l} \quad (\text{A25})$$

Then the fourth order statistics $\overline{F^4} = \overline{|F_c^{ij}|^4}, \overline{F^{i2} F^{j2}}, \overline{|F_c^{ij}|^2 F^i F^j}$ can be described by the generic equation:

$$\begin{aligned} \overline{F^4} = & \sum_k \alpha_k^{(4)} \overline{m_k^4} + \sum_k \sum_{l \neq k} \alpha_{kl}^{(3)} \overline{m_k^3} \overline{m_l} + \\ & \sum_k \sum_{l \neq k} \alpha_{kl}^{(2,2)} \overline{m_k^2} \overline{m_l^2} + \sum_k \sum_{l \neq k \neq n} \alpha_{kln}^{(2,1,1)} \overline{m_k^2} \overline{m_l} \overline{m_n} + \\ & \sum_{l \neq k \neq o \neq n} \sum_k \sum_l \alpha_{klno}^{(1)} \overline{m_k} \overline{m_l} \overline{m_n} \overline{m_o} \end{aligned} \quad (\text{A26})$$

where $\alpha_{klno}^{(1)}, \alpha_{kln}^{(2,1,1)}, \alpha_{kl}^{(2,2)}, \alpha_{kl}^{(3)}$, and $\alpha_k^{(4)}$ are given in table A1 in each specific case. **Previous equations can be**

Table A1. Coefficients of the fourth order statistics of the coherent and photometric fluxes.

	$\overline{ F_c^{ij} ^4}$	$\overline{F^{i2} F^{j2}}$
$\alpha_{k,l,n,o}^{(1)}$	$\gamma_{kl}^{ij} \gamma_{no}^{ij}$	$\beta_k^i \beta_l^j \beta_n^i \beta_o^j$
$\alpha_{kln}^{(2,1,1)}$	$2\gamma_{kk}^{ij} \gamma_{ln}^{ij} + 4\gamma_{kl}^{ij} \gamma_{kn}^{ij}$	$\beta_k^{i2} \beta_l^j + \beta_k^{j2} \beta_l^i \beta_n^i + 4\beta_k^i \beta_k^j \beta_l^i \beta_n^j$
$\alpha_{kl}^{(2,2)}$	$\gamma_{kk}^{ij} \gamma_{ll}^{ij} + 2\gamma_{kl}^{ij} \gamma_{kl}^{ij}$	$\beta_k^{i2} \beta_l^{j2} + \beta_k^i \beta_l^i \beta_k^j \beta_l^j$
$\alpha_{kl}^{(3)}$	$4\gamma_{kk}^{ij} \gamma_{kl}^{ij}$	$2\beta_k^{i2} \beta_k^j \beta_l^j + 2\beta_k^{j2} \beta_k^i \beta_l^i$
$\alpha_k^{(4)}$	$\gamma_{kk}^{ij} \gamma_{kk}^{ij}$	$\beta_k^{i2} \beta_k^{j2}$

	$\overline{ F_c^{ij} ^2 F^i F^j}$
$\alpha_{k,l,n,o}^{(1)}$	$\gamma_{kl}^{ij} \beta_n^i \beta_o^j$
$\alpha_{kln}^{(2,1,1)}$	$\gamma_{kk}^{ij} \beta_l^i \beta_n^j + \gamma_{ln}^{ij} \beta_k^i \beta_k^j + 2\gamma_{kl}^{ij} [\beta_k^i \beta_n^j + \beta_n^i \beta_k^j]$
$\alpha_{kl}^{(2,2)}$	$\gamma_{kk}^{ij} \beta_l^i \beta_l^j + \gamma_{kl}^{ij} [\beta_k^i \beta_l^j + \beta_l^i \beta_k^j]$
$\alpha_{kl}^{(3)}$	$\gamma_{kk}^{ij} [\beta_k^i \beta_l^j + \beta_l^i \beta_k^j] + 2\gamma_{kl}^{ij} \beta_k^i \beta_k^j$
$\alpha_k^{(4)}$	$\gamma_{kk}^{ij} \beta_k^i \beta_k^j$

computed knowing the statistics of m_k , that is:

$$\overline{m_k^2} = \overline{m_k}^2 + \overline{m_k} + \sigma^2 \quad (\text{A27})$$

$$\overline{p^2} = \overline{p}^2 + \overline{p} + N_{photpix} \sigma^2 \quad (\text{A28})$$

$N_{photpix}$ being the number of pixels to code the photometric outputs. The third and fourth moments $\overline{m_k^3}$ and $\overline{m_k^4}$ are derived from first and second order ones assuming Gaussian statistics for sake of simplicity.